The Journal of Chemical Physics ARTICLE scitation.org/journal/jcp

Non-equilibrium dynamics at the gas–liquid interface: State-resolved studies of NO evaporation from a benzyl alcohol liquid microjet

Cite as: J. Chem. Phys. 158, 144703 (2023); doi: 10.1063/5.0143254
Submitted: 20 January 2023 • Accepted: 13 March 2023 •
Published Online: 11 April 2023

View Online Export Citation CrossMark

Mikhail Ryazanov[1] and David J. Nesbitt[1,2,3,a)]

AFFILIATIONS

[1] JILA, National Institute of Standards and Technology and University of Colorado, Boulder, Colorado 80309, USA
[2] Department of Physics, University of Colorado, Boulder, Colorado 80309, USA
[3] Department of Chemistry, University of Colorado, Boulder, Colorado 80309, USA

[a)] Author to whom correspondence should be addressed: djn@jila.colorado.edu

ABSTRACT

First measurements of internal quantum-state distributions for nitric oxide (NO) evaporating from liquid benzyl alcohol are presented over a broad range of temperatures, performed by liquid-microjet techniques in an essentially collision-free regime, with rotational/spin–orbit populations in the $^2\Pi_{1/2,3/2}$ manifolds measured by laser-induced fluorescence. The observed rotational distributions exhibit highly linear (i.e., thermal) Boltzmann plots but notably reflect rotational temperatures (T_{rot}) as much as 30 K *lower* than the liquid temperature (T_{jet}). A comparable lack of equilibrium behavior is also noted in the electronic degrees of freedom but with populations corresponding to spin–orbit temperatures (T_{SO}) consistently *higher* than T_{rot} by ~15 K. These results unambiguously demonstrate evaporation into a *non-equilibrium distribution*, which, by detailed-balance considerations, predict quantum-state-dependent sticking coefficients for incident collisions of NO at the gas–liquid interface. Comparison and parallels with previous experimental studies of NO thermal desorption and molecular-beam scattering in other systems are discussed, which suggests the emergence of a self-consistent picture for the non-equilibrium dynamics.

Published by AIP Publishing. https://doi.org/10.1063/5.0143254

I. INTRODUCTION

It is well known that all parts of any system in thermal equilibrium obey Boltzmann distributions characterized by the same temperature.[1] Of particular relevance to the present work, this has profound implications for scattering, sticking, and evaporation of molecules at the gas–liquid interface. Specifically, since vapor-phase molecules in any thermal ensemble impinging on the liquid interface are already in thermal equilibrium with the liquid, it is tempting to think that molecules evaporating from the liquid should also have an equivalent thermal distribution with respect to all internal (vibration, rotation, and electronic) and external (translation) degrees of freedom. However, a more careful analysis[2,3] indicates that this conclusion is valid only if *all* impinging molecules interact with the liquid long enough to lose all memory of their initial state, that is, requiring *unity sticking coefficients* for all incident molecules. This assumption is overly strong and need not always be satisfied. Indeed, molecules with different collision speeds, incident angles, and rotational, vibrational, and electronic-state distributions would even be expected to have different propensities for elastic or inelastic *scattering* vs *sticking to* the surface. In fact, detailed balance only requires that evaporation produces molecules in exactly complimentary quantum state distributions with respect to scattering, maintaining a perfect balance of incoming/outgoing fluxes ($\Phi_{inc} = \Phi_{scat} + \Phi_{evap}$) with respect to each internal quantum state and velocity component. Simply stated, while the *summed* flux must recapitulate the bulk temperature, the *individual* evaporating and scattering fluxes need not be in thermal equilibrium with the liquid.[4]

This intriguing possibility of non-equilibrium dynamics at the gas–surface interface has been the topic of multiple experimental[5–10] and theoretical studies.[3,11,12] Since it is experimentally difficult to observe molecules evaporating from a liquid without collisional scrambling of these distributions in the vapor phase, much of the early research focused on desorption from metallic single crystals. In particular, the experimental studies most relevant to our current work are temperature-programmed desorption (TPD) of nitric

oxide (NO) from ruthenium[5,6] and platinum,[7,8] thermal desorption of NO from palladium upon laser heating,[9] and NO scattering from platinum.[10] In these last experiments, it is worth noting that both direct "impulsive scattering" (IS) and "trapping–desorption" (TD) can, in principle, contribute to the scattering signals detected; however, for these studies, TD proves to be the predominant channel, so the results observed largely reflect desorption dynamics. These experiments demonstrate that, depending on the surface material and temperature, the desorbing NO can be either *in* or *out of thermal equilibrium* with the surface. At sufficiently low surface temperatures (T_s), the NO molecules desorb with thermal distributions characterized by T_s. With increasing T_s, however, the translational and rotational NO temperatures continue to increase monotonically but eventually "lag" behind the surface temperature.

More recent experiments[13] have studied evaporation of atoms and small molecules from liquids with higher vapor pressures by employing the liquid-microjet technique,[14] which, by virtue of the rapid ~$1/r$ drop-off in the vapor density around the liquid microjet, can partially alleviate problems with post-evaporative collisions, but only if the microjet radius (several micrometers) is smaller than the equivalent mean free path in equilibrium vapor. For example, such experiments demonstrate that escaping Ar atoms are in close thermal equilibrium with the liquid surface (T_s), while evaporating He atoms emerge substantially *super*-Maxwellian, that is, with higher average kinetic energy than expected for T_s. Intriguingly, however, evaporating H_2 molecules appear to be *sub*-Maxwellian.[15]

Previous experiments in our group with liquid water microjets[16] aimed at studying surface dynamics for molecular NO escaping from water, but both experimental results and detailed analysis unambiguously indicate strong post-evaporative collisional effects even for the smallest water-jet radius (~2 μm) and lowest achievable supercooled water temperatures (~268 K) studied. Indeed, a model[16] that explicitly includes collisional cooling in the expanding water vapor proved to be plausibly consistent with nascent NO evaporating in thermal equilibrium with the liquid surface. However, since the NO–H_2O collisional cross section for thermal equilibration was unknown and treated as a fitting parameter, the *exact magnitude* of any collisional cooling effects remained uncertain. Most importantly, these earlier experimental results and analyses *could not rule out the possibility* of non-equilibrium evaporation, although the NO distributions were certainly impacted by post-evaporative collisions with H_2O. As a consequence, these first studies both posed and answered some questions but left the biggest question unresolved—does evaporation at the gas–liquid interface reflect an equilibrium process at the quantum-state level? The main thrust of the present work is to extend these microjet experiments to liquids for which post-evaporative collision probabilities are significantly suppressed, such that indications of non-equilibrium evaporation dynamics at the gas–liquid interface can be revealed unambiguously.

For studies of temperature dependences, it is desirable to have a solvent that remains a non-viscous liquid over experimentally feasible temperatures and yet maintains a sufficiently low vapor pressure in that range. A major problem, however, is that most liquids with low vapor pressure tend to be so viscous that forming a microjet is beyond experimental capabilities with 250 bar pressure pumps. Moreover, even if backing pressures could be increased to produce sufficient flow, frictional heating in the nozzle would substantially increase liquid temperature, thus narrowing the range of accessible microjet temperatures. In addition to these physical considerations, the solvent should be non-reactive with the dissolved NO, non-corrosive to the pumping equipment, and preferably non-poisonous.

We considered multiple inorganic and organic liquids at room temperature, ultimately choosing benzyl alcohol (BnOH) as the most promising candidate for several reasons. First of all, it is an important industrial solvent with low toxicity, relatively low vapor pressure (8 Pa ≈ 60 mTorr at 20 °C), and reasonably low viscosity (0.06 Pa s at 20 °C, i.e., only six times greater than water).[17] Furthermore, its melting point is −15 °C, allowing us to extend studies to lower temperatures than with water microjets. Finally, the elevated boiling point (205 °C) provides access to high temperatures as well, since even at 50 °C, the vapor pressure of BnOH (<100 Pa) is still six times lower than of water at its triple point.[17] From a chemical perspective, BnOH is aromatic alcohol, with an OH group to incorporate some hydrogen-bonding solvent properties relevant to water. In addition to low toxicity and tolerable odor, benzyl alcohol is compatible with polytetrafluorethylene (PTFE) and polyether ether ketone (PEEK) plastic seals and does not corrode stainless steel. Miscibility with methyl alcohol (MeOH) and partial miscibility with water makes system purging and cleanup simple. Finally, NO dissolves in but does not react with BnOH. Although we were unable to find direct information on NO solubility in BnOH, it can be estimated from NO solubilities in, for example, ethanol and toluene,[18] both of which are an order of magnitude higher than NO solubility in water. Thus, even though NO diffusion, which ultimately limits NO evaporative flux from the microjet,[16] is arguably slower in BnOH than in water, this is more than compensated by higher dissolved NO concentrations to produce sufficiently strong NO signals from BnOH microjets.

II. EXPERIMENT

The experimental setup for the present work is largely based on the apparatus from our previous water-microjet study[16] and, thus, can be described briefly, highlighting only the most important differences. A high-vacuum chamber, pumped out by a turbomolecular pump through a liquid-nitrogen cryogenic baffle, contains (see Fig. 1) a quartz microjet nozzle mounted on a three-axis translational stage, entrance and exit light baffles for the excitation laser, and a photomultiplier assembly for detection of the laser-induced fluorescence (LIF). At the bottom of the vacuum chamber, the microjet is collected in a glass bottle submerged in liquid nitrogen.

The solution preparation procedure is essentially the same, replacing water with benzyl alcohol (Alfa Aesar, ACS-grade, purity ≥99%) and passing NO from the gas cylinder through a liquid-nitrogen–methanol trap to remove NO_2 contamination. Although the NO solubility in benzyl alcohol is not accurately known, we estimate (see above) that 2.7 bar (2,000 Torr) equilibrium NO pressures correspond to ~50 mM NO concentrations (~10^{-3} molar fraction). After preparation, this NO/BnOH solution is transferred from the mixing cylinder to the syringe pump and kept under high pressure during the course of experiments.

The liquid-delivery system was modified by replacing the valves with higher-pressure models (Swagelok SS-4SKPS2 and SS-83XPS2), allowing the use of the full pressure range of the syringe pump (up

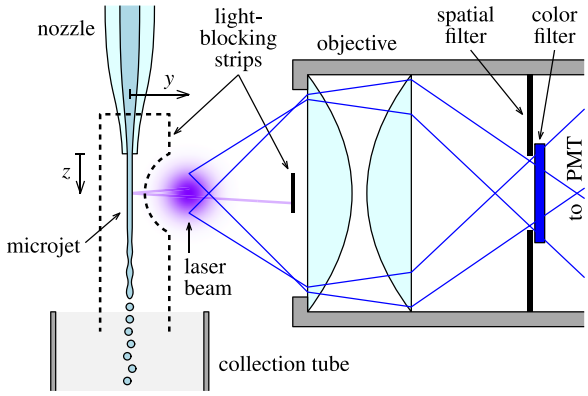

FIG. 1. Schematic drawing of the experimental arrangement (not to scale). The downstream distance *z* is measured vertically from the nozzle exit. The distance *y* from the jet is measured horizontally from the jet axis.

to 258 bars), which is essential for forming microjets with more viscous liquids. Especially important is a three-way value for switching the nozzle line between the syringe pump containing the NO/BnOH solution and a purging cylinder supplying MeOH at 30 bars for purging the nozzle between experiments. This system provides continuous flow of the liquid through the nozzle, greatly reducing clogging problems. The process of a complete switch between the working and purging liquids takes ~30 min, as determined by monitoring the NO LIF signal and microjet parameters such as flow rate and laminar length, both of which differ significantly between MeOH and BnOH.

Other modifications are related to the liquid temperature control. The HPLC filter used in the water microjet experiments[16] was replaced by a short HPLC guard column (Idex C-130B, 2 mm × 2 cm), packed with gold powder for more efficient heat transfer. The resulting ~50 μl internal volume at typical ~100 μl/min flow rates leads to ~30 s residence times, sufficient for complete temperature equilibration of the solution with the filter body. A resistance temperature detector (RTD), in addition to the thermocouple (TC) at the filter center, is attached to the filter body near the nozzle mount for redundant temperature readout and monitoring gradients along the filter during temperature adjustments. The temperature of the "coolant" (ethanol or ethanol–water mixture) pumped through the coil soldered to the filter body[16] is controlled by water-cooled Peltier modules (TE Technology HP-199-1.4-1.15). These can be powered in the forward or reverse direction to provide both cooling and heating, thereby allowing continuous control of the filter temperature between −24 °C and at least +50 °C. This experimental upper limit arises from safety concerns about the reliability of plastic seals separating the high-pressure liquid from high vacuum.

Compared to previous water-microjet experiments, the BnOH microjet diameter is increased twofold, to ∅8.5 ± 0.1 μm (nozzles made from New Objective SilicaTips electrospray emitters with a nominal ∅10 μm), in order to enable the formation of a microjet with the more viscous BnOH liquid. During the experiments, the backing pressure was adjusted between 35 and 258 bars to compensate for the temperature-dependent viscosity and maintain the flow rate at 110 μl/min (except at the lowest temperature, −23 °C, where the flow dropped to 90 μl/min at the highest available pressure; see Fig. S1 in the supplementary material), corresponding to a 32 m/s jet speed. The laminar flow length of the microjet, before the breakup due to the Rayleigh–Plateau instability, is also temperature-dependent, varying between 2 mm at +50 °C and 4.5 mm at −23 °C.

Major improvement in LIF measurement capabilities is obtained by upgrading the 10 Hz laser system previously shared with the room-temperature ionic liquid (RTIL) and molten-metal scattering experiments[19,20] to a new laser system consisting of a Nd:YAG pump laser (Continuum Surelite II) operating at 20 Hz and a double-grating dye laser with a built-in frequency-tripling unit (Radiant Dyes NarrowScan). The doubled repetition rate allows scanning the relevant NO spectral range from 44 040 to 44 500 cm^{-1} with 0.02 cm^{-1} steps in about 20 min, with typically at least two scans performed consecutively under the same experimental conditions to confirm reproducibility. To ensure linearity of the LIF response, room-temperature spectra for a static NO fill ($5 \cdot 10^{-6}$ mbar, similar to NO evaporant density from the microjet, in 0.13 mbar He buffer) have been recorded and analyzed over a range of laser pulse energies and, as a result, 1 μJ was chosen for all reported measurements. During each scan, this pulse energy is stabilized by automatically adjusting the Nd:YAG pump power, resulting in < 10% pulse-to-pulse RMS variation and no long-term drift.

A final significant improvement involves blocking the excitation laser light scattered by the microjet and nozzle from reaching the LIF-detector PMT. Although the laser beam is spatially filtered to a nearly Gaussian shape before entering the vacuum chamber, ~0.5% of the energy is still distributed into diffraction rings surrounding the central spot. When scattered from the microjet and nozzle, the intensity of this weak light can, nevertheless, easily exceed the LIF signal intensity from the much lower-density evaporating NO. Even though ≳90% of the excitation light is blocked by a color filter, the remaining fraction can still cause transient overloading of the PMT. Thus, in previous experiments, the laser beam (with a ~0.5 mm half-intensity radius) had to be positioned at least 2 mm from the microjet. These problems are largely eliminated in the present work by the addition of two light-blocking strips. The first strip, schematically shown as a dashed contour in Fig. 1, reduces the amount of stray laser light hitting the nozzle and microjet, without affecting the central Gaussian part of the laser beam. The second is a 4 mm wide strip running horizontally (only cross section visible in Fig. 1) across the front of the LIF-collecting objective. This strip completely blocks the predominantly horizontal line of the laser light scattered from a vertical cylindrical microjet, while discarding only ~10% of LIF radiation reaching the lens. Experiments confirm the effectiveness of both these measures, which allows us to perform LIF measurements almost two times closer to the microjet (at 1.2 mm), despite its twofold larger diameter.

III. RESULTS

A typical LIF spectrum of NO evaporating from the BnOH microjet is shown in Fig. 2. As the new laser system is different from the previous one,[16] the line shape used in the spectral fitting procedure had to be modified. An empirical form reasonably reproducing the experimental data was found to be a weighted sum of a narrow Gaussian $\exp[-x^2/(2\sigma^2)]$ and a wider two-sided exponential

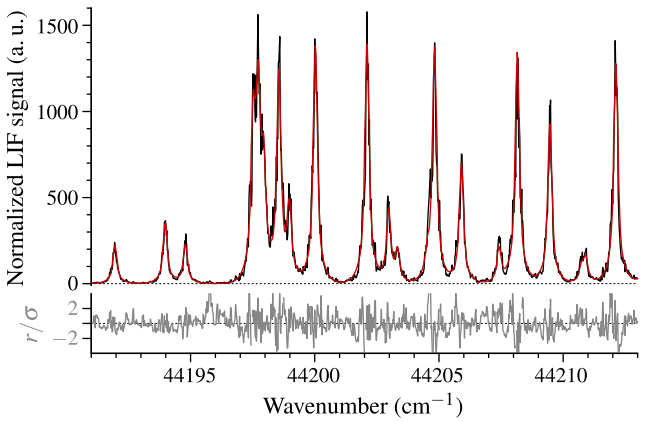

FIG. 2. A small sample region of the full LIF spectrum for NO evaporating from a ∅8.5 μm BnOH microjet (17 °C filter temperature, laser at z = 1 mm downstream, and y = 1.2 mm from the jet). The black line shows the experimental fluorescence intensity normalized to the laser pulse energy, the red line shows the best fit, and the gray line below shows the normalized residuals.

(Laplace distribution) $\exp(-|x|/\gamma)$. As before, all lines in the spectrum share the globally fit width parameters σ and γ and the ratio of Gaussian/Laplace contributions, with relative quantum state populations obtained from integrated intensities of the corresponding spectral lines. Careful inspection of Fig. 2 reveals that normalized residuals are less random than in the previous work,[16] but the fit quality is, nevertheless, quite sufficient for extracting reliable NO populations.

Similar to our previous studies with water microjets,[16] the extracted quantum-state populations in each spin–orbit manifold (see Figs. S5 and S6 in the supplementary material) are indistinguishable within experimental uncertainty from an identical Boltzmann distribution of rotational levels. The data for each spin–orbit manifold are, therefore, combined to yield a single rotational temperature (T_{rot}) in further analysis. However, the effective spin–orbit temperatures (T_{SO}), obtained from integrated populations in each manifold, are routinely different from the rotational temperatures. As mentioned above, several spectra were recorded under each experimental condition (filter temperature T_{f} and flow rate), all demonstrating high levels of reproducibility (see Fig. S7 in the supplementary material). Thus, in Fig. 3, we present averaged results and statistical uncertainties calculated from all data taken at each liquid temperature.

Interestingly, the overall positive correlation of the *total* evaporating NO signal [Fig. 3(a)] with the BnOH temperature is qualitatively similar to previous observations in water microjets.[16] This is almost certainly due to the temperature dependence of the NO diffusion coefficient in liquid BnOH, which limits the NO escape rate from the microjet. However, we are unaware of any reports on temperature-dependent diffusion rates for of NO in BnOH, and thus, no quantitative comparison can be offered at this time.

On the other hand, the NO rotational and spin–orbit temperatures [Fig. 3(b)] show quite promising trends *opposite* to what was observed for water microjets, now *positively* (instead of negatively) *correlated* with filter temperature. However, for a truly quantitative comparison of NO rotational and spin–orbit temperatures with the

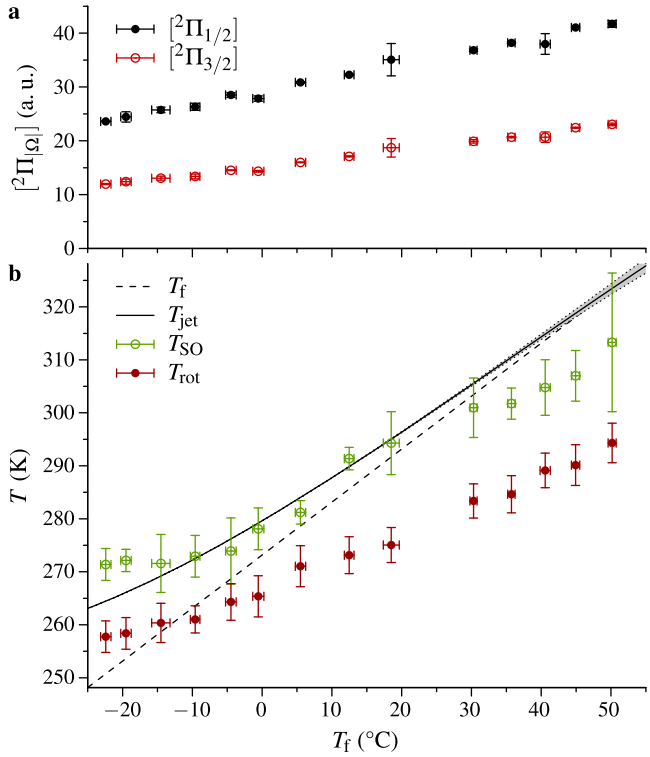

FIG. 3. Spin–orbit populations {$[^2\Pi_{1/2}]$ and $[^2\Pi_{3/2}]$, panel (a)} and rotational and spin–orbit temperatures [T_{rot} and T_{SO}, panel (b)] of NO evaporating from a ∅8.5 μm BnOH microjet, measured at z = 1 mm and y = 1.2 mm, for various filter temperatures T_{f}. The error bars encompass fitting uncertainties and run-to-run variations (at least two runs are performed for each T_{f} setting). The simulated microjet temperature T_{jet}, including frictional heating and evaporative cooling, is shown for comparison by the black line for z = 1 mm; the gray dotted region indicates the range of estimates evaluated over the $0 \le z \le 2$ mm range.

liquid-surface temperature, we must take into account two additional effects. The first is frictional heating of BnOH as it passes through the nozzle. This heating is much stronger than for water due to the much higher viscosity and lower heat capacity of BnOH[17] and varies from 1.5 K at the highest filter temperature to 12 K at the lowest (see Fig. S2 in the supplementary material). The second contribution is due to evaporative cooling of the microjet propagating in vacuum. Interestingly and in stark contrast to water, this effect is now almost negligible due to the much lower vapor pressure and specific heat of evaporation of BnOH,[17] reaching only −0.6 K at the highest filter temperature (see Fig. S3 in the supplementary material). The combined impact of these two additional effects on T_{jet} is plotted (solid line) in Fig. 3 as a function of the experimentally controlled filter temperature T_{f}.

Finally, we tested for possible signal contamination by background NO scattered from colder or warmer parts of the vacuum chamber by horizontally moving the nozzle to y = 10 mm from the microjet. Such an eightfold lateral displacement resulted in a fivefold drop in the overall LIF intensity but with no change in the fitted NO rotational and spin–orbit temperatures. Thus, we are confident that any effects due to background NO are negligible within our reported experimental uncertainties.

IV. DISCUSSION

A. Estimation of collisional cooling

In a previous water-microjet study,[16] we also observed NO rotational temperatures significantly lower than the liquid-surface temperature. However, it was also expected that for water microjets even of the smallest experimentally feasible radius, collisions in the vapor could not be suppressed completely. Thus, we developed a simple analytical model for post-evaporative rotational cooling of NO molecules by inelastic collisions with adiabatically expanding water vapor. Notably, this model was able to fit the experimental results remarkably well, assuming that NO molecules evaporate in thermal equilibrium with the water surface and then cool in collisions with the co-expanding water vapor, with a modest rotational relaxation cross section ($\sigma \sim 13$ Å^2).

While the BnOH vapor pressures are much lower, the collisional cross sections are expected to be larger; we, therefore, might still expect some collisional effects. Based on the same modeling described in the water-microjet studies, Fig. 4 displays the experimentally measured NO rotational temperature as a function of the microjet surface temperature compared with predictions of our collisional-cooling model, again assuming NO evaporation in thermal equilibrium and calculated for a range of rotational relaxation cross sections. The plots immediately reveal two important facts. First of all, a broad comparison of trends is qualitatively poor and completely different from the excellent agreement obtained in the water-microjet studies. Second, to even qualitatively attribute the magnitude of these observed temperature differences to collisional cooling, the inelastic cross sections would need to be at least an order of magnitude larger (>100 Å^2). More importantly, however, the experimental and predicted model dependences exhibit completely *different shapes*, such that even if we assume cross sections large enough to reproduce the magnitude of experimental temperature differences, the correlations between T_{rot} and T_{jet} would be negative (as observed for water) instead of positive.

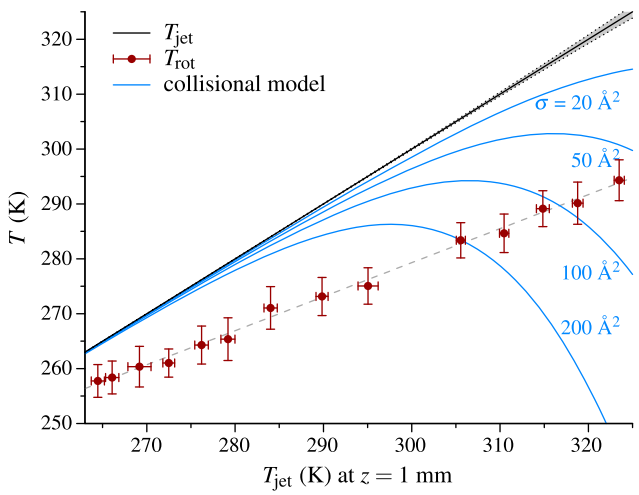

FIG. 4. Comparison of the experimental rotational temperatures with the predictions of the collisional-cooling model assuming thermal equilibrium at the microjet surface, plotted for various effective collisional cross sections σ. Most importantly, no value of σ even qualitatively reproduces the experimental results, which, therefore, provide the first evidence for non-equilibrium evaporation dynamics. The gray dotted region shows the predicted range of microjet temperatures between 0 and 2 mm downstream. The dashed gray line is a linear dependence $T_{rot} = 0.62\ T_{jet} + 93$ K fitted to the experimental data points.

We can, therefore, conclude that the measured asymptotic NO rotational temperatures are inconsistent with evaporation in thermal equilibrium and subsequent collisional cooling, but instead must arise from non-equilibrium evaporation dynamics at the liquid surface. The post-evaporative collisional effects are negligible (assuming physically reasonable inelastic cross sections), except maybe at the highest surface temperatures. It is worth emphasizing, however, that such a collision-cooling model assumes that the vapor behaves as an adiabatically expanding ideal gas. This, in turn, requires sufficient collisions among the evaporating BnOH molecules, an assumption that might not hold even at the highest microjet temperatures, where BnOH vapor pressures are still relatively low. Therefore, the expanding BnOH vapor is likely to cool less than our simple model predicts, thus making any cooling effects on the NO co-evaporant molecules even more negligible.

B. Comparison with other systems

From Fig. 4, the observed dependence of NO rotational temperatures T_{rot} on microjet temperatures T_{jet} appears to be remarkably linear (slope ~0.62) over the experimental range sampled. This empirical simplicity might at first seem surprising, but, in fact, very similar behavior has been previously observed in several other systems and merits some discussion. Perhaps the most relevant are the experimental studies of NO temperature-programmed desorption (TPD) from solid metals. Although a metallic crystal face is obviously quite different from a liquid surface, the crucial parallel is that adsorbed/dissolved NO molecules in both experiments spend minutes to hours in contact with the substrate and, thus, are rigorously in thermal equilibrium with it until they desorb/evaporate. Nevertheless, NO thermally desorbing from a Ru(001) surface at $T_s = 455 \pm 20$ K exhibits a Boltzmann rotational distribution with a significantly lower rotational temperature $T_{rot} = 235 \pm 35$ K,[5] and a similarly low translational temperature $T_{||} = 235 \pm 45$ K.[6] Moreover, similar studies of NO desorbing from Pt(111) at several surface temperatures[7,8] again yielded cleanly Boltzmann rotational distributions, but with an interesting transition from "equilibrium" to "non-equilibrium" behavior depending on the surface temperature. Specifically, for the lowest temperatures (up to $T_s \approx 200$ K), NO desorbs with $T_{rot} \approx T_s$ (similar to sublimation of solid NO films at 50 K[21]), but beyond $T_s \gtrsim 300$ K, the desorbing NO exhibits T_{rot} values systematically lower than T_s. Experiments[9] with laser heating of NO adsorbed on Pd(111) to $T_s = 1100 \pm 100$ K also yielded NO thermally desorbing in a Boltzmann rotational distribution, but with $T_{rot} = 640 \pm 40$ K, i.e., again much lower than T_s.

Molecular-beam scattering experiments arguably offer far better control of initial quantum states and access to a broader range of surface temperatures, but their interpretation in terms of *desorption* requires the additional assumption that all incident molecules stick to the surface and fully accommodate before leaving (i.e., "trapping–desorption" mechanism). This assumption is likely to be justified for scattered molecules yielding diffuse angular distribution and zero dependence on incident angles and energies. Studies[10] of

NO scattering from a Pt(111) surface over T_s = 200–890 K demonstrated such diffuse and angle/energy-independent behaviors, with the quantum-state populations consistent with TPD studies on NO/Pt(111)[7,8] but now extendable to much higher temperatures that permit examination of the dependence of T_{rot} on T_s. The results show that, for $T_s \lesssim 300$ K, the scattered NO emerges with $T_{rot} \approx T_s$, while at higher $T_s \gtrsim 300$ K, the NO rotational temperature starts to deviate linearly from T_S with a local slope $dT_{rot}/dT_s \sim 1/4$, qualitatively similar to the NO evaporation behavior observed in the present work. The authors of these early scattering studies interpreted their results as the effect of temperature-dependent NO surface coverage and incomplete rotational accommodation at higher surface temperatures. In our case, however, NO coverage of the liquid surface is negligible at any temperature, and, although the evaporating NO molecules might not spend a long time *at the surface*, they were surely equilibrated *with the bulk liquid*.

Of the greatest relevance to the present microjet studies, there have also been quantum-state-resolved scattering experiments with *low-vapor-pressure liquids* demonstrating a similarly clean linear T_{rot} dependence on T_s. For example, in NO scattering from a room-temperature ionic liquid (RTIL) surface,[19] a distinctly linear dependence of T_{rot} on T_s was observed for the trapping–desorption (TD) channel, with the slope ~0.6, this time even qualitatively matching the present NO evaporation results. It is worth noting that in these RTIL studies, not only was the spin–orbit ratio *not in equilibrium* with T_s, but also the two spin–orbit manifolds had different rotational temperatures, although with the same dT_{rot}/dT_s slope. Interestingly, T_{rot} for the upper spin–orbit manifold was even *higher* than T_s at the lower range of liquid temperatures studied. In these experiments, however, the incident NO energy was high enough (E_{inc} = 2.7 kJ/mol ≈ 940 cm^{-1}) to leave ample excess energy (for comparison, $kT \approx 200$ cm^{-1} at $T \approx 300$ K) even after excitation into the upper spin–orbit manifold ($\Delta E_{SO} \approx 123$ cm^{-1}).[22] Furthermore, it was noted that both the conductive and charged nature of the RTIL surface could be responsible for additional non-adiabatic electronic effects due to electron transfer into a transient anionic $NO^-(^3\Sigma)$ state.[19]

Interestingly, high-resolution infrared Doppler rotation/translation studies of low-energy scattering of CO (closed-shell but otherwise similar to NO) from various organic liquids (PFPE, squalane, and glycerol)[23] also reveal a remarkably linear dependence of both T_{rot} and T_{trans} on T_s, now with slopes $dT_{rot,\,trans}/dT_s \sim 0.5$ and independent of any obvious physical properties of the liquids. Similar to the present work, the measured CO distributions emerged in each case systematically colder than T_s over a wide range of temperatures. The observed gap between $T_{rot,\,trans}$ and T_s decreases at lower temperatures, but the experimental range sampled was insufficient to determine whether the linear behavior would continue, in principle, eventually leading to non-equilibrium behavior in reverse order (i.e., $T_{rot/trans} > T_s$), or, more likely, smoothly transitioning to equilibrium behavior with $T_{rot} \approx T_{trans} \approx T_s$.

C. Theoretical considerations

Several simple theoretical models have been proposed for the variety of non-equilibrium behaviors observed in the aforementioned experiments. Unfortunately, while such models qualitatively rationalize some of the measurements, none even qualitatively reproduces our present results. For example, models assuming that molecules transiently attached to the surface have constrained angular motion and that these constraints non-adiabatically disappear on desorption always predict non-Boltzmann final-state distributions, with an enhanced rotational tail and, thus, always "hotter" than T_s.[24] Alternatively, models that assume molecules at the surface to be free 2D rotors (constrained to in-plane rotation) that adiabatically become 3D rotors with internal energy shuffled but conserved upon desorption[25] predict $T_{rot} \approx T_s/2$, which yields a reasonable dT_{tr}/dT_s slope but fails to account for the fact that T_{rot} approaches T_s at some finite, non-zero temperature. Yet, a third model assumes that molecules at the surface are nearly free 3D rotors, and desorption occurs by adiabatic partial conversion of their rotational energy to out-of-plane translation required to overcome the potential barrier.[26] Such a model predicts markedly non-Boltzmann distributions, this time with a high-J tail corresponding to T_s but with the low-J states substantially over-populated, neither feature of which is evident in the present experiments.

On the other hand, numerical classical trajectory simulations for simple model potentials can reproduce previous experimental results quite well. For example, simulations of NO scattering from Ag(111) and Pt(111)[27] yield Boltzmann-like rotational distributions with $T_{rot} \approx T_s$ below some threshold T_s and then a linear dependence of T_{rot} on T_s with a sub-unity slope. Agreement with the experiment is nearly quantitative, though the model-potential parameters have been optimized for the best reproduction of the data. Nevertheless, the number of free parameters was small, and their fitted values were consistent with general expectations. Moreover, the authors noted that the fitted potentials cannot be considered accurate because their predicted temperatures are not very sensitive to fine details of the potentials. From our perspective, this is good news and suggests that the observed dynamical behavior may be more general rather than specific to a particular choice of molecule/crystal scattering system.

Similarly, numerical simulations of low-energy CO scattering from liquids with classical molecular dynamics in *ab initio*-based model potentials were also able to reproduce experimental results remarkably well.[23] The theoretical simulations have been performed over a much broader T_s range than experimentally accessible and, interestingly, yielded a roughly linear dependence of T_{rot} on T_s without any transition to $T_{rot} \approx T_s$ behavior at the lowest surface temperatures. As a result, the simulations predict T_{rot} in excess of T_s by as much as 50 K at sufficiently low surface temperatures. Curiously, this excess CO thermal energy (rotational plus translational, $\frac{5}{2}k\Delta T \sim 1$ kJ/mol for $\Delta T \sim 50$ K) at the lowest T_s in these simulations, in fact, even exceeds the incident CO kinetic energy.[23] Such a "super-thermal" scattering might appear surprising at first sight but is really no more so than "sub-thermal" scattering. The only difference is that, while at higher surface temperatures, the state-dependent sticking coefficient for faster and rotationally excited CO molecules is lower than for CO with lower translational and rotational energies, this dependence could be biased in the opposite direction for lower T_s. In any event, such behavior does not violate the first and second laws of thermodynamics in terms of detailed balance and quantum-state-dependent sticking coefficients.[2,3]

While coarse theoretical modeling[28] and indirect experimental evidence[29,30] suggest that the BnOH liquid surface is composed mostly of benzene rings, we are not aware of any studies regarding

NO–BnOH interactions, even in the gas phase. Therefore, performing any numerical simulations of NO evaporation from liquid BnOH would require efforts beyond the scope of the present experimental studies. We hope, however, that our results will spark interest in studying this system theoretically, and in addition to reproducing them in numerical simulations, the general similarities leading to such non-equilibrium behavior in various systems discussed above will be discovered.

D. Empirical models

The current evidence for *rotationally non-equilibrated evaporation* of NO from a liquid is, to the best of our knowledge, unprecedented, and for which any *analytic* theoretical description of the energy-transfer dynamics remains elusive. In the hopes of stimulating further theoretical progress, however, we can offer the following empirical models.

If the sticking coefficients are considered phenomenologically, it is easy to show that in order to obtain a state distribution that is *also Boltzmann* but with *a different rotational temperature*, the sticking coefficient must have an exponential dependence on rotational energy,

$$S(E) = \frac{p_{\mathrm{expt}}(E)}{p_{\mathrm{eq}}(E)} \sim \frac{\exp\left(-E/kT_{\mathrm{rot}}\right)}{\exp\left(-E/kT_{\mathrm{jet}}\right)} = \exp\left[-\frac{E}{k}\left(\frac{1}{T_{\mathrm{rot}}} - \frac{1}{T_{\mathrm{jet}}}\right)\right] = \exp\left(-\frac{E}{kT_0}\right),$$

where $T_0 = \left(T_{\mathrm{rot}}^{-1} - T_{jet}^{-1}\right)^{-1}$ is some characteristic temperature describing the energy scale for the rotational-state dependence of the sticking coefficient.[9] Note that T_0 is not necessarily directly related to any other energetic characteristics of the system, in particular, $T_0 \to \infty$ in the equilibrium case with $T_{\mathrm{rot}} \approx T_{\mathrm{jet}}$. So far, T_0 can be considered simply as a fitting parameter, but if it is known, the evaporant rotational temperature could be predicted for any microjet temperature from $T_{\mathrm{rot}} = \left(T_{\mathrm{jet}}^{-1} + T_0^{-1}\right)^{-1}$.

The simplest assumption would be that T_0 does not depend on the surface temperature at all. Examples of such NO rotational temperature dependences for several assumed T_0 values are shown in Fig. 5 together with experimental data for comparison. As evident in Fig. 5, this model correctly predicts a smooth transition from $T_{\mathrm{rot}} \approx T_{\mathrm{jet}}$ at very low microjet temperatures to $T_{\mathrm{rot}} < T_{\mathrm{jet}}$ at higher T_{jet}. However, no single T_0 value quantitatively reproduces the experimental dependence of T_{rot} on T_{jet}. Specifically, while $T_0 \approx 4000$ K may match the average temperature deviations, the predicted slope in the experimental T_{jet} range is quite wrong, so that T_{rot} is significantly underestimated at the lowest T_{jet} and overestimated at the highest. On the other hand, the $T_0 \approx 1000$ K predictions match the linear slope in the relevant range but underestimate all experimental T_{rot} values by ~100 K.

Such discrepancies clearly indicate that T_0 must depend on T_{jet}. Furthermore, if we calculate T_0 for all experimental T_{jet} and corresponding T_{rot} values (see Fig. 6), we see that this dependence is quite strong, exhibiting ~threefold variation over the experimental range explored. While shamelessly empirical, Fig. 6 summarizes our attempts to fit the observed dependence with some simple functions (for which we currently have neither intuitive pictures nor compelling physical motivation):

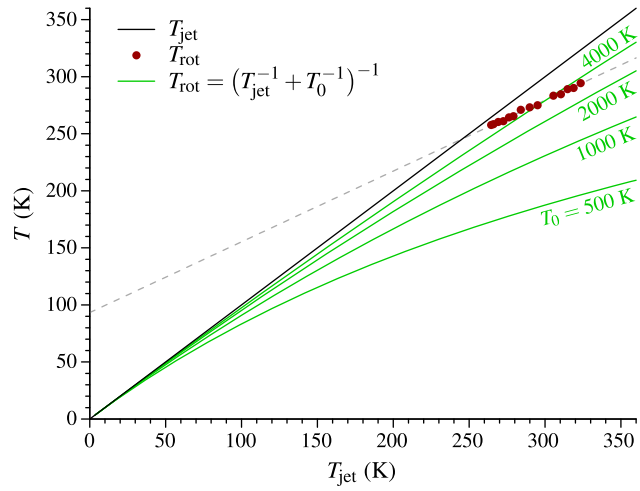

FIG. 5. Comparison of the experimental rotational temperatures T_{rot} with the predictions of the model assuming exponentially decreasing sticking coefficient[9] with a constant characteristic temperature T_0, plotted for various T_0 values. The dashed gray line is the same as in Fig. 4.

- Linear dependence of inverse temperature: $T_0^{-1} = T_{(0)}^{-1} + \alpha T_{\mathrm{jet}}$, with two adjustable parameters $T_{(0)}$ and α. This dependence predicts negative values of T_0 for low T_{jet}, which would imply sticking coefficients exponentially *growing* with rotational energy. To satisfy $S(E) \leq 1$, however, this growth range must be limited, meaning that $S(E)$ is exponential only at low energies but must saturate or even decrease at high energies, where quantum-state populations drop significantly.
- Hyperbolic dependence: $T_0 = T_{\mathrm{lim}} + \alpha/(T_{\mathrm{jet}} - T_c)$, with three adjustable parameters—limiting value T_{lim}, scale factor α, and critical surface temperature T_c.

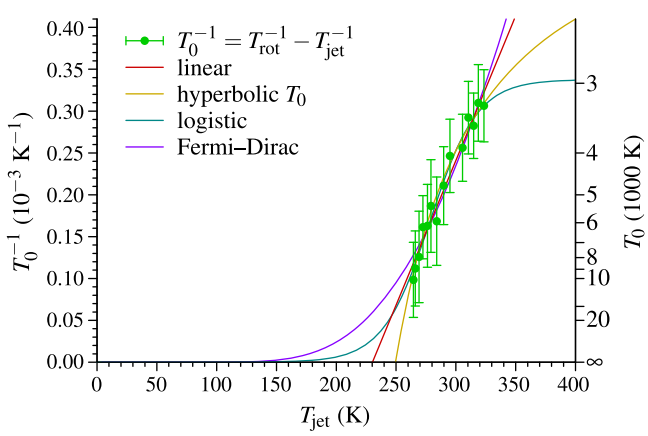

FIG. 6. Inverse characteristic temperatures $T_0^{-1} = T_{\mathrm{rot}}^{-1} - T_{\mathrm{jet}}^{-1}$ for each experimental data point and several empirical fitting curves (see text for details).

- Logistic-function dependence: $T_0^{-1} = T_{max}^{-1}/(1 + \exp[(T_c - T_{jet})/T_w])$, with three adjustable parameters—upper limit T_{max}, transition temperature T_c, and width T_w.
- Fermi–Dirac function dependence: $T_0^{-1} = T_{max}^{-1}/[\exp(T_c/T_{jet}) + 1]$, with two adjustable parameters—upper limit T_{max} and characteristic temperature T_c.

The dependence of T_{rot} on T_{jet} predicted by these empirical models is shown in Fig. 7, each matching available data within experimental uncertainties but extrapolating to dramatically different and often non-physical behaviors outside the experimental range. For example, the "linear T_0^{-1}" model predicts $T_{rot} \gtrsim T_{jet}$ for $T_{jet} < 250$ K and a reversed order $T_{rot} < T_{jet}$ for $T_{jet} > 250$ K. The model predicts a curious local maximum in T_{rot} at $T_{jet} \sim 500$ K and is asymptotically unphysical with $T_{rot} \to 0$ as $T_{jet} \to \infty$. The "hyperbolic T_0" model behaves reasonably at $T_{jet} \gtrsim 250$ K, predicting monotonic T_{rot} growth up to some asymptotic limit, but diverges completely unphysically at $T_{jet} \sim 200$ K. The "logistic" model, with T_0^{-1} smoothly varying from 0 to $T_{max} \sim 3000$ K over a relatively narrow range of microjet temperatures, predicts $T_{rot} \approx T_{jet}$ up to $T_{jet} \sim 200$ K, above which T_{rot} deviates from T_{jet} almost linearly and then slowly levels off, asymptotically approaching $T_{rot} = T_{max}$ as $T_{rot} \to \infty$. The "Fermi–Dirac" model exhibits an equivalent behavior at low T_{jet}, but, similarly to the "linear T_0^{-1}" model, predicts T_{rot} to drop at $T_{jet} \gtrsim 400$ K, although to a finite value instead of 0.

While each of these empirical fits adequately describes the experimental data, the T_{jet} range studied is simply insufficient to make any meaningful distinctions between them. However, outside the studied T_{jet} range, they make quite different predictions, which potentially can be experimentally tested. What is clearly needed are more physically motivated theoretical models for the functional dependence of T_{rot} on T_{jet} in order to extract further insight into the microscopic evaporation dynamics.

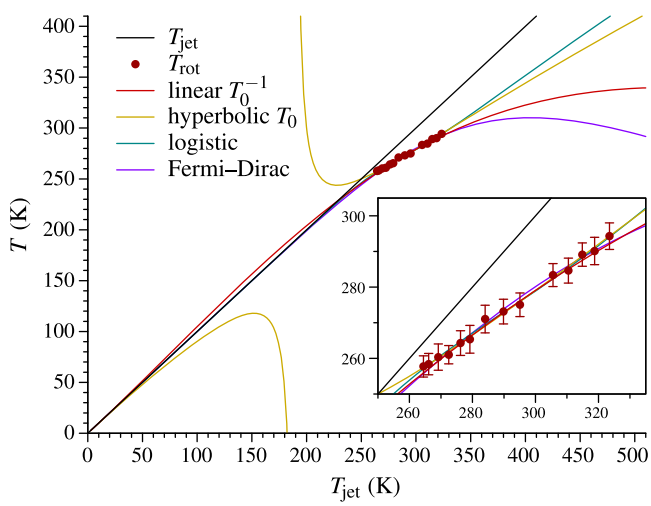

FIG. 7. Rotational temperatures T_{rot} predicted by various empirical models for the dependence of T_0 on T_{jet} (see Fig. 6). The inset shows a blow-up of the experimentally studied region.

E. Final remarks

Experimentally, the T_{jet} range could be extended to somewhat higher temperatures, but already at 350 K, BnOH vapor pressure becomes comparable to water vapor pressure at its freezing point, and thus, collisional effects, clearly evident in our previous water-microjet studies,[16] are expected to play a significant role and complicate the analysis. Extension to lower microjet temperatures would be more interesting, as the linear T_{rot} trend seen in Figs. 4 and 5 should cross the $T_{rot} = T_{jet}$ line at 245 K, only 20 K below the studied range. While it is below the BnOH freezing temperature, it might be possible to supercool the liquid. However, the BnOH viscosity rises tremendously at low temperatures, demanding much higher pressures to push the liquid through the microjet nozzle. In addition, this increases the frictional heating in the nozzle (see Fig. S2 in the supplementary material), which in turn would require supercooling by much more than 20 K. A switch to a larger-diameter nozzle (made possible by lower vapor pressures at lower temperatures) could potentially solve this problem but is beyond the scope of the present work.

So far, we have focused only on rotational non-equilibrium effects, but a few words can also be said about spin–orbit temperatures. As seen from Fig. 3, T_{SO} is everywhere greater than T_{rot} by ~15 K or ~5%, although the limited temperature range and measurement accuracy do not allow us to conclude whether this is a constant offset, a constant ratio, or something else. Unlike T_{rot}, the effective spin–orbit temperature T_{SO} dependence actually does cross the T_{jet} line, with $T_{SO} > T_{jet}$ at the lowest surface temperatures. However, in contrast to T_{rot}, which is extracted from highly redundant population distributions over many tens of individual states, T_{SO} is essentially determined from a single population ratio $[^2\Pi_{3/2}]/[^2\Pi_{1/2}]$. Consequently, deviations of T_{SO} from T_S could, in principle, simply reflect unknown shifts in spin–orbit energies for NO dissolved in BnOH and inefficient spin–orbit equilibration during the molecular escape event. Alternatively interpreted from a detailed-balance perspective, the NO evaporant would unambiguously exhibit such non-equilibrium spin–orbit populations if sticking coefficients for NO impinging on a BnOH liquid surface were different for $^2\Pi_{1/2}$ and $^2\Pi_{3/2}$ spin–orbit states. It is interesting to note that in previous studies[21] of NO sublimation at $T_s = 50 \pm 3$ K, despite the otherwise expected "equilibrium" picture in terms of rotations ($T_{rot} \approx T_s$) and a $\cos\theta$ angular flux distribution, spin–orbit temperatures $T_{SO} = 70 \pm 12$ K noticeably higher than T_s were found, which was putatively attributed to exactly such a spin–orbit dependence of sticking coefficients.

Finally, we note that the experimental measurements performed in the present studies have so far provided no information on *translational* distributions. However, if NO evaporation from the BnOH microjet surface is "rotationally mediated," then strong coupling between (hindered) rotational and translational degrees of freedom during molecular evaporation should lead to a correlation between translational and rotational energies, which would affect rotational-state *flux* distributions. We perform quantum-state-resolved *density* measurements, and the flux–density relationship in turn depends on state-specific speed distributions.[31–33] That is, if a sufficiently strong correlation exists, our measured rotational distributions might be biased. To overcome this problem, future experiments with resonance-enhanced multiphoton ionization (REMPI) of NO with subsequent time-of-flight measurements are possible

and would provide velocity distribution for each quantum state, thus allowing one to both explore these rotation–translation correlations and reveal a more detailed picture of equilibrium vs non-equilibrium dynamics in rotation/translation/spin–orbit degrees of freedom.

V. CONCLUSION

Benzyl alcohol has a vapor pressure that is too high to study evaporation dynamics with bulk planar samples, but at the same time, sufficiently low such that we were able to study evaporation of dissolved NO from a BnOH microjet in an essentially collision-free regime. The results unambiguously demonstrate that NO evaporant emerges *rotationally colder* than the BnOH liquid surface, with the temperature difference increasing approximately linearly from −8 K at $T_{jet} \approx 265$ K to as much as −30 K by $T_{jet} \approx 325$ K. These results are unique in the sense that this is the first time that rotationally non-equilibrated evaporation from a liquid surface has been conclusively demonstrated and reported. Interestingly, however, these results closely resemble similar findings in other experiments based on NO thermal desorption and scattering from metallic single crystals, as well as NO and CO scattering from low-vapor-pressure liquids. While numerical simulations are beyond the scope of the present work, such simulations have proven quite successful for the interpretation of previous experimental studies. Specifically, they have shown that even classical trajectory simulations with relatively simple model potentials can reproduce such "rotational cooling" effects, in some cases even semi-quantitatively. However, we are aware of no *conceptual* theoretical model proposed to date that properly describes these non-equilibrium effects and, in particular, makes quantitative predictions for the dependence of T_{rot} on the surface temperature T_s. Nevertheless, the remarkable similarity between results for such diverse systems as evaporation, desorption, and scattering of NO and CO from conductive and non-conductive single crystals and liquids suggests that such behaviors must be closely related and, someday, theoretically derivable from general physical principles. It is our hope that these microjet studies have contributed toward stimulating further experimental and theoretical interest into deeper elucidation of the underlying physics for such fascinating yet complex non-equilibrium gas–liquid interfacial phenomena.

SUPPLEMENTARY MATERIAL

See the supplementary material for additional plots of experimental conditions, estimated microjet frictional heating and evaporative cooling, Boltzmann plots, and raw results extracted from LIF spectra fitting.

ACKNOWLEDGMENTS

Funding for this work was provided by the National Science Foundation under Grant No. CHE-1665271/2053117 from the Chemical, Structure, Dynamics and Mechanisms-A Program, with additional support for apparatus construction from PHY-1734006 (Physics Frontier Center Program) and the Air Force Office of Scientific Research (FA9550-15-1-0090). Company identifications in the text are solely for clarity and do not represent JILA/NIST support for specific vendors.

AUTHOR DECLARATIONS

Conflict of Interest

The authors have no conflicts to disclose.

Author Contributions

Mikhail Ryazanov: Data curation (equal); Formal analysis (equal); Investigation (lead); Software (lead); Validation (lead); Writing – original draft (lead); Writing – review & editing (equal). **David J. Nesbitt**: Conceptualization (lead); Data curation (equal); Funding acquisition (lead); Project administration (lead); Resources (lead); Supervision (lead); Writing – review & editing (equal).

DATA AVAILABILITY

The data that support the findings of this study are available from the corresponding author upon reasonable request.

REFERENCES

[1] D. A. McQuarrie, *Statistical Thermodynamics* (University Science Books, Sausalito, 2000).
[2] R. D. Levine and R. B. Bernstein, *Molecular Reaction Dynamics and Chemical Reactivity* (Oxford University Press, Oxford, 1987).
[3] J. C. Tully, "The dynamics of adsorption and desorption," Surf. Sci. **299–300**, 667 (1994).
[4] G. Comsa and R. David, "Dynamical parameters of desorbing molecules," Surf. Sci. Rep. **5**, 145 (1985).
[5] R. R. Cavanagh and D. S. King, "Rotational- and spin-state distributions: NO thermally desorbed from Ru(001)," Phys. Rev. Lett. **47**, 1829 (1981).
[6] D. S. King and R. R. Cavanagh, "State selected velocity measurements: NO/Ru(001) thermal desorption," J. Chem. Phys. **76**, 5634 (1982).
[7] D. S. King, D. A. Mantell, and R. R. Cavanagh, "NO thermally desorbed from a saturation coverage on Pt(111): Internal state distributions," J. Chem. Phys. **82**, 1046 (1985).
[8] D. A. Mantell, R. R. Cavanagh, and D. S. King, "Internal states distributions of NO thermally desorbed from Pt(111): Dependence on coverage and co-adsorbed CO," J. Chem. Phys. **84**, 5131 (1986).
[9] J. A. Prybyla, T. F. Heinz, J. A. Misewich, and M. M. T. Loy, "Direct observation of rotational cooling in thermal desorption: NO/Pd(111)," Surf. Sci. **230**, L173 (1990).
[10] J. Segner, H. Robota, W. Vielhaber, G. Ertl, F. Frenkel, J. Häger, W. Krieger, and H. Walther, "Rotational state populations of NO molecules scattered from clean and adsorbate-covered Pt(111) surfaces," Surf. Sci. **131**, 273 (1983).
[11] N. Shenvi, S. Roy, and J. C. Tully, "Nonadiabatic dynamics at metal surfaces: Independent electron surface hopping," J. Chem. Phys. **130**, 174107 (2009).
[12] N. Shenvi, S. Roy, and J. C. Tully, "Dynamical steering and electronic excitation in NO scattering from a gold surface," Science **326**, 829 (2009).
[13] J. A. Faust and G. M. Nathanson, "Microjets and coated wheels: Versatile tools for exploring collisions and reactions at gas–liquid interfaces," Chem. Soc. Rev. **45**, 3609 (2016).
[14] M. Faubel, S. Schlemmer, and J. P. Toennies, "A molecular beam study of the evaporation of water from a liquid jet," Z. Phys. D. **10**, 269 (1988).
[15] D. K. Lancaster, "Inert gas scattering and evaporation from jet fuel surrogates using liquid microjets," Ph.D. thesis, University of Wisconsin, 2014.

[16]M. Ryazanov and D. J. Nesbitt, "Quantum-state-resolved studies of aqueous evaporation dynamics: NO ejection from a liquid water microjet," J. Chem. Phys. **150**, 044201 (2019).
[17]K. Kroenlein, C. D. Muzny, A. F. Kazakov, V. Dijky, R. D. Chirico, J. W. Magee, I. Abdulagatov, and M. Frenkel, https://wtt-pro.nist.gov (2012).
[18]C. L. Young, *Oxides of Nitrogen, Solubility Data Series* (Pergamon Press, 1981).
[19]A. Zutz and D. J. Nesbitt, "Nonadiabatic spin–orbit excitation dynamics in quantum-state-resolved NO($^2\Pi_{1/2}$) scattering at the gas–room temperature ionic liquid interface," J. Phys. Chem. C **119**, 8596 (2015).
[20]A. Zutz, K. A. Peterson, and D. J. Nesbitt, "Nonadiabatic dynamics at the gas–molten metal interface: State-to-state resolved scattering of NO from hot gallium (600–1000 K)," J. Phys. Chem. C **125**, 341 (2021).
[21]D. F. Padowitz and S. J. Sibener, "Sublimation of nitric oxide films: rotational and angular distributions of desorbing molecules," Surf. Sci. **217**, 233 (1989).
[22]G. Herzberg, *Spectra and Molecular-Structure.1. Spectra of Diatomic-Molecules* (Princeton University Press, Princeton, NJ, 1968).
[23]T. A. Livingston Large and D. J. Nesbitt, "Low-energy CO scattering at the gas-liquid interface: Experimental/theoretical evidence for a novel subthermal impulsive scattering (STIS) channel," J. Phys. Chem. C **124**, 28006 (2020).
[24]J. W. Gadzuk, U. Landman, E. J. Kuster, C. L. Cleveland, and R. N. Barnett, "Infinite conical well: An analytic model for quantum mechanical hindered rotors," Phys. Rev. Lett. **49**, 426 (1982).
[25]S. E. Bialkowski, "A statistical interpretation of the rotational temperature of NO desorbed from Ru(001)," J. Chem. Phys. **78**, 600 (1983).
[26]J. M. Bowman and J. L. Gossage, "Rotational cooling of rigid rotors desorbed from flat surfaces," Chem. Phys. Lett. **96**, 481 (1983).
[27]C. W. Muhlhausen, L. R. Williams, and J. C. Tully, "Dynamics of gas–surface interactions: scattering and desorption of NO from Ag(111) and Pt(111)," J. Chem. Phys. **83**, 2594 (1985).
[28]J. Dietter and H. Morgner, "Structure and dynamics at the liquid surface of benzyl alcohol," Chem. Phys. **241**, 55 (1999).
[29]R. E. Ballard, G. G. Gunnell, and W. P. Hagan, "Photoelectron spectroscopic and thermodynamic studies of the free surface of benzyl alcohol," J. Electron Spectrosc. Relat. Phenom. **16**, 435 (1979).
[30]G. Andersson, "Angle resolved ion scattering spectroscopy at surfaces of pure liquids: Topography and orientation of molecules," Phys. Chem. Chem. Phys. **7**, 2942 (2005).
[31]W. W. Harper, S. A. Nizkorodov, and D. J. Nesbitt, "Quantum state-resolved reactive scattering of F + CH_4 → HF(v,J) + CH_3: Nascent HF(v,J) product state distributions," J. Chem. Phys. **113**, 3670 (2000).
[32]W. W. Harper, S. A. Nizkorodov, and D. J. Nesbitt, "Differential scattering dynamics of F + CH_4 → HF(v,J) + CH_3 via high-resolution IR laser dopplerimetry," Chem. Phys. Lett. **335**, 381 (2001).
[33]W. W. Harper, S. A. Nizkorodov, and D. J. Nesbitt, "Reactive scattering of F + HD → HF(v,J) + D: HF(v,J) nascent product state distributions and evidence for quantum transition state resonances," J. Chem. Phys. **116**, 5622 (2002).